Particle Accelerators
1973, Vol. 4, pp. 229–238

PARTICLE DISTRIBUTION IN A STEEL BEAM STOP FOR 28 GeV PROTONS†

G. W. BENNETT, H. N. BROWN, H. W. J. FOELSCHE, J. D. FOX, D. M. LAZARUS, G. S. LEVINE

Brookhaven National Laboratory, Upton, New York 11973, USA

and

T. E. TOOHIG

National Accelerator Laboratory, Batavia, Illinois 60510, USA

R. H. THOMAS

Lawrence Berkeley Laboratory, Berkeley, California 94720, USA

J. KOSTOULAS

University of Rochester, Rochester, New York 14627, USA

The distribution of energetic particles in a steel beam stop has been measured using ^{11}C activation of polyethylene. The axial data extends to a depth of 3.1 kg/cm^2. The axial attenuation length beyond the build-up is 156 ± 1.1 g/cm^2. Results are compared with previous beam stop experiments.

1. INTRODUCTION

Previous studies[1–3] have explored the distribution of secondary hadron flux in beam stops for incident proton beams of 6 GeV and higher. We present here the distribution of hadrons in a steel beam stop to extend the previous results to higher energy and greater axial depth in the stop using presently available beams of much higher intensity and negligible contamination.

The overall layout is shown in Fig. 1; details of the upstream end of the stop are shown in Figs. 2 and 3. The overall length was 12 m, a typical transverse dimension was 1.5 m. The stop consisted of plates or blocks of steel with axial separation of 7.5 cm to allow instrumentation to be inserted. The upstream plates were 5 cm thick, intermediate pieces 10–30 cm thick, the 18 downstream blocks were 60 cm thick. Each block was weighed to determine its density. The 5 cm pieces were rolled plates and had a density of 7.7 g/cm^3, all the other units were 7.0 g/cm^3. For convenience during the experiment the upstream face of each piece was lettered consecutively; a list of the parameters of the beam stop is given in Table I.

† Work performed under the auspices of the U.S. Atomic Energy Commission.

2. EXPERIMENTAL PROCEDURE

Polyethylene foils 2.5 cm wide, 10 cm high and 0.1 mm thick were arrayed horizontally at beam height in each slot. Center-to-center separation of the foils near the axis was 2.5–5 cm, increasing to 20 cm at 60 cm from the beam axis. These foils were taped to a fiber board strip 10 cm high by 1.2 m wide, suspended at beam height. Deep in the stack 'chunks' of plastic scintillator material (100 gram right circular cylinders of Pilot B) were used to increase the sensitivity.

Beam intensity for each run was monitored by means of polyethylene foils, wide enough to intercept all of the incident protons in the beam at the 'C' target location. Data were collected in three runs of about ten minutes duration, each at successive depths. The scintillator chunks have a different response from the foils used for beam and fluence monitoring, principally due to their different geometry and counting efficiency. The correction was established by exposing foils and chunks simultaneously in one run at intermediate depths in the stack.

Beam intensity averaged about 10^{12} protons per pulse with a 2.4 sec repetition period. Autoradiographs of the beam monitor foils showed the

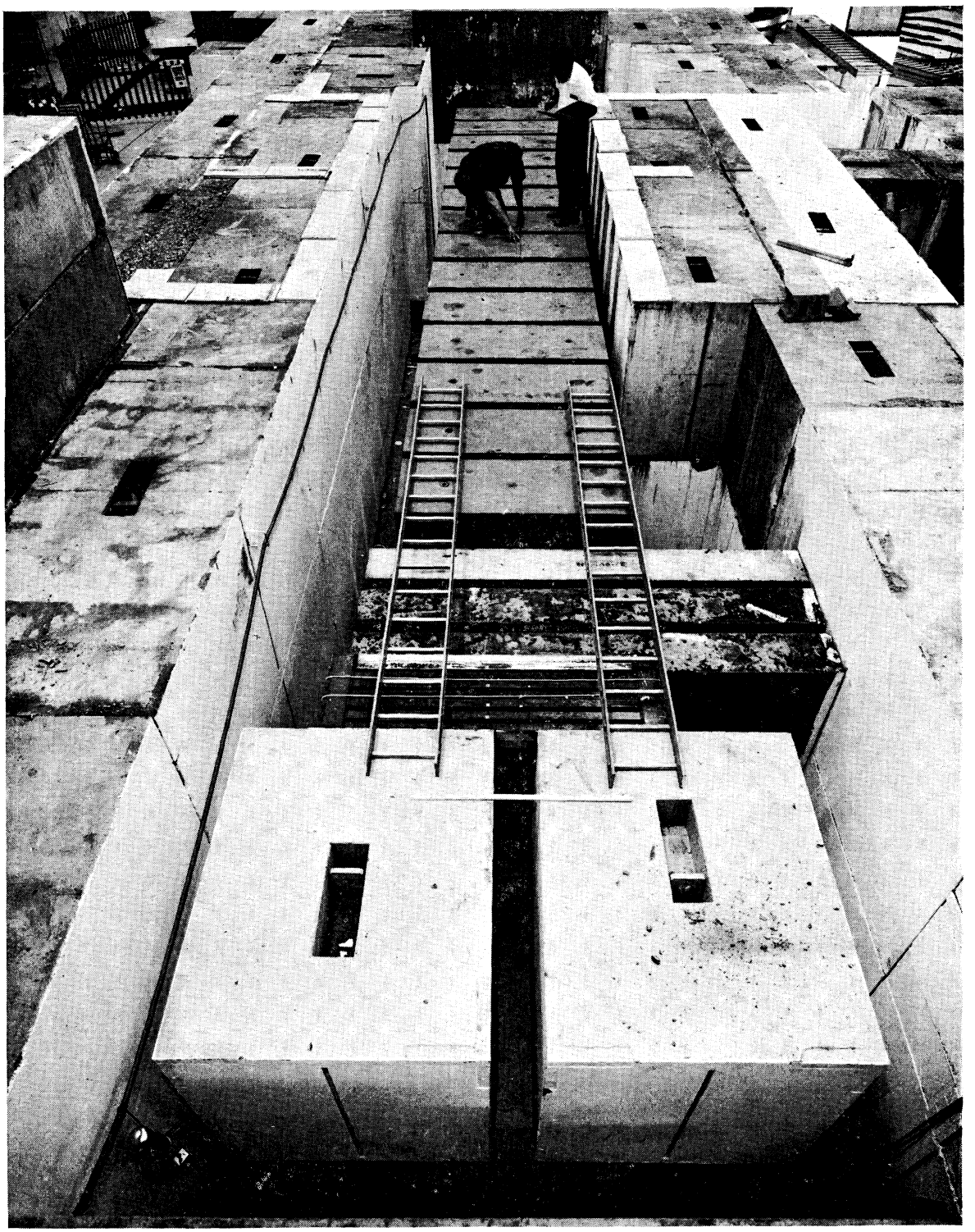

FIG. 1. View of beam stop from above the 'C' target location. Concrete blocks in foreground are omitted from Figs. 2 and 3.

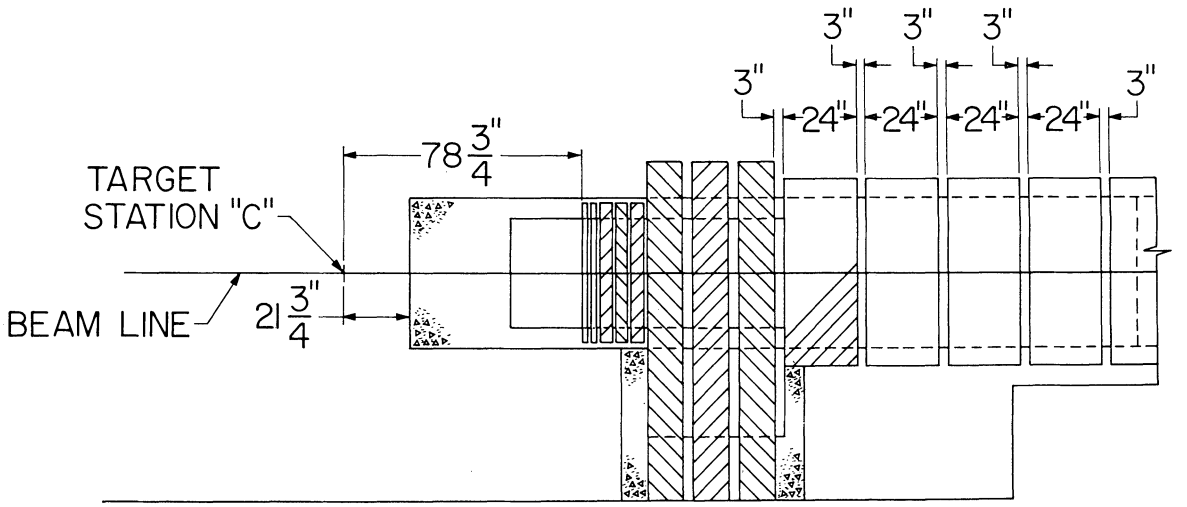

FIG. 2. Plan view of upstream section of stop.

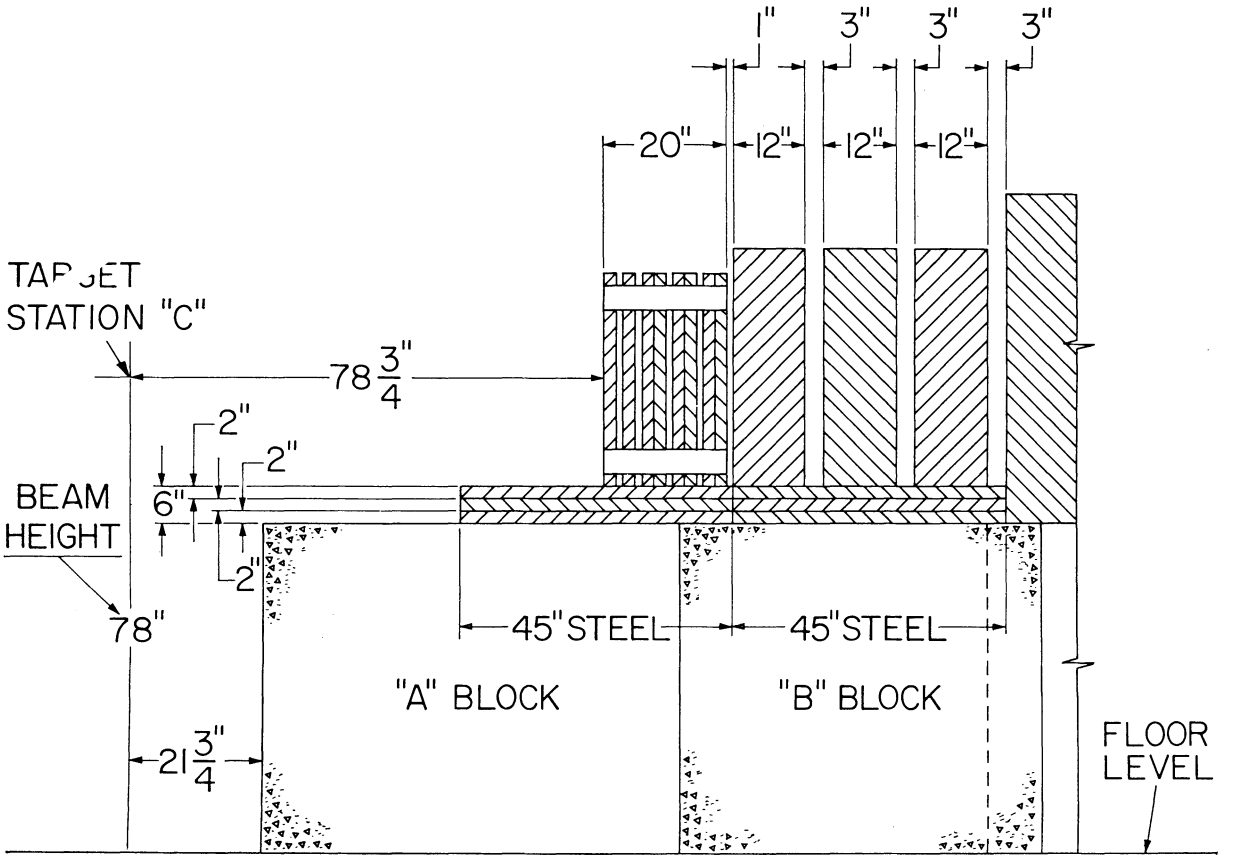

FIG. 3. Side view of upstream section of beam stop.

TABLE I

Beam stop parameters

Slot	Upstream block thickness cm	Running thickness cm	ρ of block g/cm^3	Block thickness g/cm^2	Running thickness g/cm^2	Energy to 'range out' (GeV)
A	0	0.		0	0	
B	5.25	5.25		40.7	40.7	
C	5.25	10.5	7.76	40.7	81.4	
D	10.5	21.0		81.5	162.9	
E	10.5	31.5		81.5	244.4	
F	10.5	42.0		81.5	325.9	
G	30.5	72.5	7.06	215.3	541.2	
H	30.5	103.0	7.06	215.3	756.5	1.21
I	30.5	133.5	6.96	212.3	968.8	1.57
J	61.3	194.8	7.01	429.7	1398.5	2.3
K	61.3	256.1	6.76	414.4	1812.9	3.0
L	61.3	317.4	6.98	427.9	2240.8	3.8
M	61.3	378.7	6.98	427.9	2669.0	4.6
N	61.3	440.0	6.91	423.6	3092.0	5.3
O	61.3	501.3	6.91	423.6	3516.0	6.1
P	61.3	562.6	6.98	427.9	3944.0	6.9
Q	61.3	623.9	7.05	432.2	4376.0	7.8
R	61.3	685.2	7.05	432.2	4808.0	8.5
S	61.3	746.5	6.98	427.9	5236.0	9.4
T	61.3	807.8	7.05	432.2	5668.0	10.3
U	61.3	869.1	7.01	429.7	6096.0	11.1
V	61.3	930.4	7.01	429.7	6526.0	11.9
W	61.3	991.7	6.80	416.8	6943.0	12.6

horizontal and vertical semi-axes of the beam to be 3 mm and 6 mm respectively at the 'C' target location; the horizontal and vertical emittance of the beam is 0.157 π and 0.094 π cm mrad.[4]

3. DATA ANALYSIS

The relative fluence across the foils is given by

$$RA = \frac{[(C-B)/W]\exp(t/\tau)}{A_m[(C_m-B_m)/W_m]\exp(t_m/\tau)}$$

where C = counts per unit time of foil in well counter at time t

t = Time at start of well counting relative to beam exposure time

B = well counter background counts per unit time

τ = ^{11}C mean lifetime (29.47 minutes)

A_m = area of beam monitor foil

W = foil weight,

and the subscript m identifies beam monitor foil quantities.

This procedure minimizes systematic errors, particularly uncertainty in counter efficiency and corrections due to fluctuations in beam intensity during irradiation. The quantity RA (relative activity) is then identical to the number of secondary particles per square centimeter in the detector foils per proton on the monitor foil, assuming that the cross section for ^{11}C production is the same for the secondaries as for the primary protons. Carbon-eleven in any case has a constant excitation function[5] from $\sim$300 MeV to the highest energy of interest in this investigation.

Near the axis the size of the foils was large compared to a characteristic dimension of the particle distribution so systematic resolution was unfolded by fitting to a multiparameter function. For each set of foils at a given axial depth in the stack the data were fitted to a function

$$\Phi(x) = \exp\left(\sum_{i=0}^{n} a_i x\right)$$

(where x is the transverse distance from the beam axis) such that

$$\chi^2 = \sum_{j=1}^{L}\left[RA_j - \int_{\text{foil}} (x_j)\,dS\right]^2 = \text{minimum.}$$

Here RA_j is the relative activity at x_j, L is the number of foils at that depth, and the surface integral is over the area of the detector foils. The polynomial of order $n = 5$ (6 parameters) was found to give the best fits. The fitting program was repeated for different assumed origins ($x = 0$) scanning in steps of 2 mm. The center giving the best χ^2 was selected for each plane.

The geometric correction for finite foil size was significant only near the beam axis where the fluence, $\Phi(x)$, changes rapidly within the foil dimensions. The correction was less than 5 per cent at distances greater than 3 cm from the beam axis.

A least square fitting procedure was also used to evaluate the attenuation length in the steel for various angular trajectories.

4. RESULTS AND DISCUSSION

Isofluence contours are displayed in Fig. 4. The characteristic 'flame' pattern is similar to the results obtained at Berkeley[1] for a concrete beam stop with 6 GeV incident proton energy. The details of the distribution are shown in Figs. 5 and 6 where the fluence versus transverse position is shown for each slot depth; only one side of each distribution is shown. These profiles are similar to those reported from CERN[2] for 9.1 and 18.2 GeV incident protons, in which the track density of

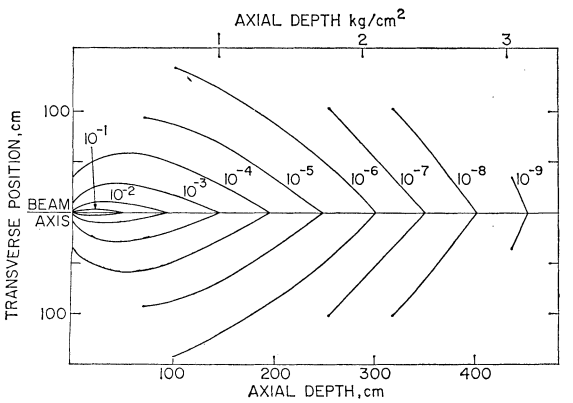

FIG. 4. Isofluence contours in the beam stop. Curves are designated in units of particles per cm² per proton incident.

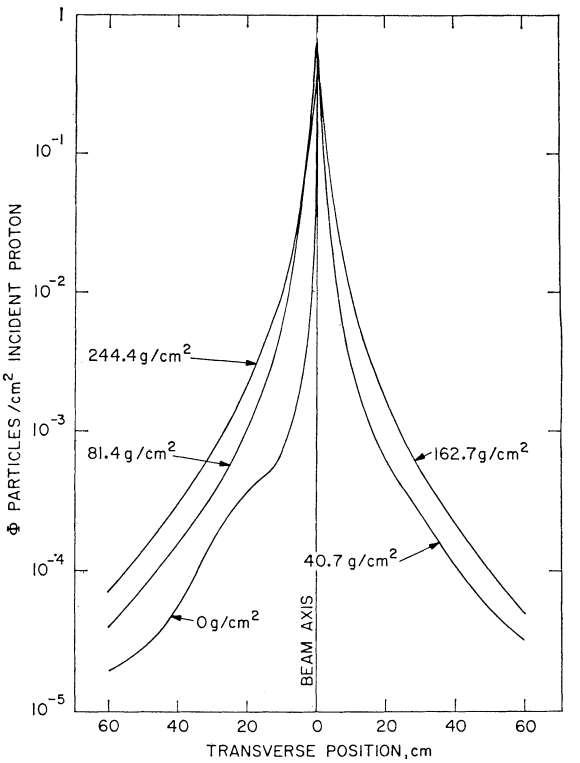

FIG. 5. Transverse fluence distributions for slots near the upstream section of the stop.

secondaries in nuclear emulsions was measured. Baarli *et al.*[2] report ^{11}C results but those data are not extensive.

The 'raw' data are given in Table II as values of Relative Activity (RA) defined above. Note that these data are not corrected for the geometry and size of detectors—they represent the average of the secondary distribution over the area of each detector foil.

The general shape of the hadron field in the stop is summarized in Fig. 7, showing the transverse full width at half maximum and at one-tenth maximum, of the energetic secondaries, as a function of axial depth. Figure 8 is a plot of fluence, for a given angle with respect to the beam axis, against the radial distance through the stack from the point of intersection of the beam axis on the face of the beam stop. The shallow region shows a departure from simple exponential attenuation, presumably due to build-up. The solid portion of each curve is the fit to exponential absorption, $\Phi \sim e^{-r/\lambda}$. The attenuation length, λ, is seen to be nearly indepen-

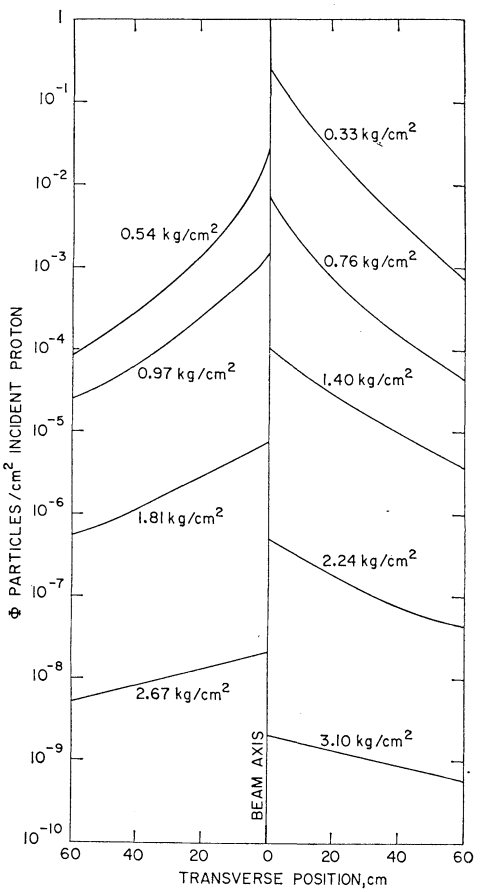

FIG. 6. Transverse fluence distributions at intermediate depths.

dent of angle as Fig. 9 shows. The zero degree plot gives the most significant fit statistically for the attenuation length, $\lambda_0 = 156.0 \pm 1.1$ g/cm^2. The weighted fit for all angles is $\lambda = 153.6 \pm 1.0$ g/cm^2, not very different. This bears out the basic premise of the Moyer model,[6] an absorption length invariant with angle and invariant with energy in the equilibrium region beyond build-up.

Figure 10 displays the integral of the fitted fluence function over the cross-sectional area of the beam stop at each slot in the stack, fitted to an exponential decay. The upstream data were ignored in the fit since the hadron cascade is building up in the front plates and the attenuation does not become dominant until a depth of 30 cm. This is the 'build-up distance' to the maximum of the integrated flux. (See Fig. 11 for definitions.) The length of the 'transition region', the distance to the point where the integral flux is equal to that at the front surface, is 115 cm. The multiplicity, defined as the maximum number of secondaries per incident proton normalized to the zero depth value, is found from Fig. 10 to be 11.6 ± 0.8. The 'build-up factor', the integral fluence extrapolated from the equilibrium region to the front face normalized to the measured value at the front face is found to be 60 ± 4. The relaxation length for the integral flux is $\Lambda = 197 \pm 3$ g/cm^2. It should be noted that the integral flux scale of Fig. 10 is absolute, and not the result of normalization. The value at the face of the stop for the integral of all the flux is 2.5 particles per proton incident. This allows a total of 1.5 back-scattered secondaries from the beam stop per proton, giving one confidence in the data treatment.

The attenuation length for the integral flux,

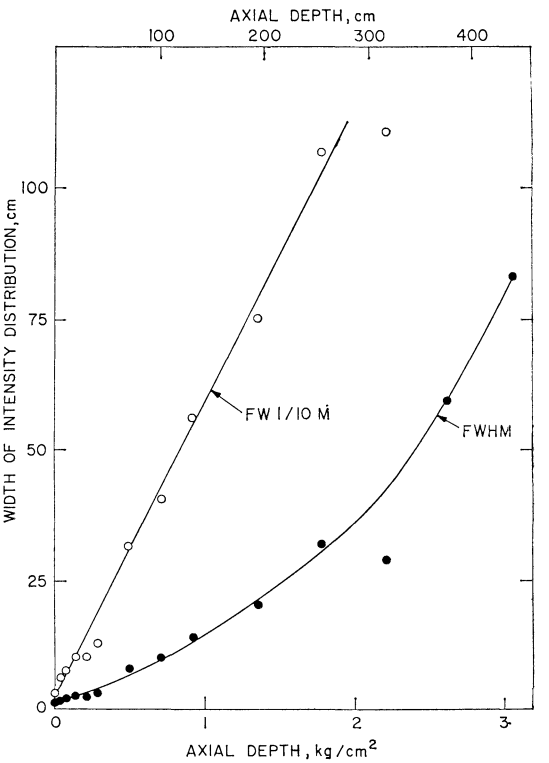

FIG. 7. Full width at half maximum and full width at one-tenth maximum of the transverse fluence distribution *vs.* axial depth in the stop.

TABLE II

Experimental data—RA† (secondaries per sq cm per beam proton)

Transverse‡ displacement cm	Slot A Run 2	B 2	C 2	D 2	E 3	F 3	G 3	H 3	I 3	J 3	K 3
−61	2.30E-5	3.66E-5	4.52E-5	6.39E-5	7.76E-5	9.33E-5	1.09E-4	6.51E-5	2.84E-5	4.30E-6	8.56E-7
−40.6	6.92E-5	1.19E-4	1.60E-4	2.54E-4	3.29E-4	3.88E-4	3.76E-4	1.99E-4	8.38E-5	1.12E-5	1.22E-6
−20.3	3.53E-4	6.76E-4	1.27E-3	2.08E-3	2.76E-3	2.88E-3	1.95E-3	8.90E-4	3.20E-4	3.44E-5	3.59E-6
−10.2	1.12E-3	3.64E-3	7.94E-3	1.25E-2	1.40E-2	1.23E-2	6.03E-2	2.21E-3	7.36E-4	6.79E-5	6.66E-6
− 7.6	1.71E-3										
− 5.1	2.67E-3	1.90E-2	3.51E-2	5.03E-2	4.82E-2	3.77E-2	1.23E-2	4.08E-3	1.19E-3	9.38E-5	7.51E-6
− 2.5	3.64E-2										
0	1.01E-2	8.09E-2	1.10E-1	1.02E-1	1.17E-1	8.72E-2	1.73E-2	5.33E-3	1.43E-3	1.08E-4	8.55E-6
2.5	2.16E-3										
5.1	1.43E-3	6.49E-3	1.22E-2	1.86E-2	2.27E-2	2.34E-2	8.17E-3	2.92E-3	9.12E-4	8.17E-5	6.85E-6
7.6	9.76E-4										
10.2	7.00E-4	2.11E-3	3.93E-3	5.48E-3	8.35E-3	8.69E-3	4.42E-3	1.69E-3	5.76E-4	5.48E-5	5.95E-6
20.3	2.50E-4	5.36E-4	8.81E-4	1.35E-3	1.93E-3	2.19E-3	1.56E-3	6.74E-4	2.61E-4	2.86E-5	3.20E-6
40.6	5.37E-5	1.00E-4	1.36E-4	1.99E-4	2.61E-4	3.15E-4	3.16E-4	1.57E-4	7.17E-5	1.01E-5	1.51E-6
61.0	1.98E-5	3.04E-5	3.93E-5	5.00E-5	7.02E-5	8.53E-5	9.58E-5	5.22E-5	2.68E-5	3.88E-6	8.98E-7

Transverse‡ displacement cm	Slot G Run 4	H 4	I 4	J 4	K 4	L 4	K 5	L 5	M 5	N 5
−61.0	9.65E-5	5.50E-5	2.51E-5	3.65E-6	5.11E-7					
−40.6	3.31E-4	1.69E-4	7.09E-5	9.16E-6	9.57E-7		8.06E-7	8.13E-8	8.42E-9	9.55E-10
−20.3	1.72E-3	7.42E-4	2.66E-4	2.69E-5	2.46E-6		2.51E-6	1.87E-7	1.31E-8	1.42E-9
−10.2			6.10E-4	5.09E-5	4.42E-6					
− 5.1	1.06E-2	3.15E-3	9.63E-4	7.08E-5	5.44E-6	3.59E-7				
0	1.49E-2	4.21E-3	1.10E-3	7.91E-5	6.08E-6	4.08E-7	6.61E-6	4.37E-7	2.07E-8	1.93E-9
5.1	6.77E-3	2.47E-3	7.30E-4	6.11E-5	5.23E-6	4.04E-7				
10.2				4.42E-5						
20.3	1.33E-3	6.04E-4	4.60E-4	2.38E-5			2.21E-6	1.75E-7	1.39E-8	1.72E-9
40.6	2.54E-4	1.41E-4	5.93E-5	8.03E-6						
61.0	8.10E-5	4.64E-5		3.29E-6	4.55E-7		3.88E-7	4.21E-8	5.25E-9	6.27E-10
34.0	4.16E-4	2.05E-4								
54.3	1.13E-4	6.65E-5								
74.6	6.34E-5	2.14E-5								
84.7	3.11E-5	1.31E-5								
94.9	1.30E-5	8.12E-6								
115.3		3.38E-6								
135.5	3.08E-6	1.50E-6								
155.9	2.39E-6	8.30E-7								

† RA is defined in the text; notation used: 2.30E-5 = 2.30×10^{-5}

‡ Displacement relative to nominal beam axis.

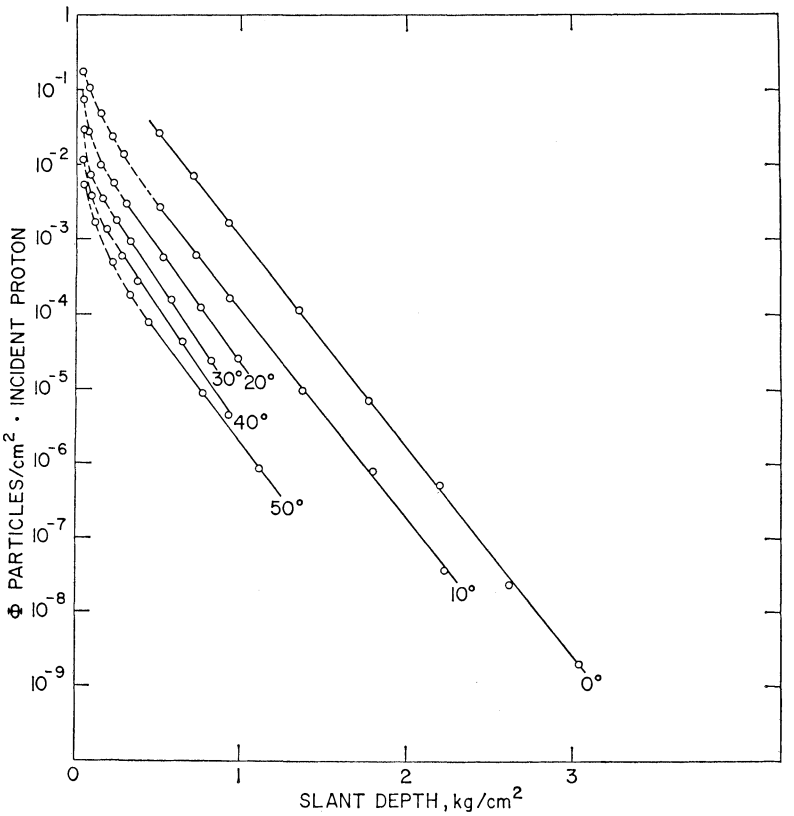

FIG. 8. Fluence *vs.* radial distance measured from point of incidence in steel for various angles with respect to the beam axis.

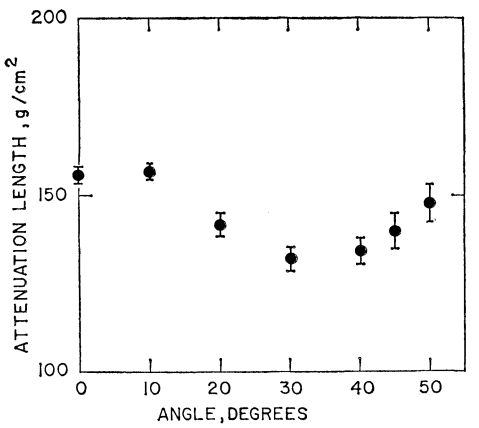

FIG. 9. Attenuation length, λ, for the solid curves of Fig. 8.

$\Lambda = 197 \pm 3$ g/cm^2, is a measure of the removal of particles by interaction with the steel, and may be related to the total absorption cross section for hadron—iron nucleus interactions by

$$\sigma_a = \frac{A}{N_0 \Lambda} = 471 \pm 7 \text{ mb}$$

where A is the atomic weight of iron, N_0 is Avogadro's number. Since Λ is determined at a depth in the stack greater than 800 g/cm^2 it is reasonable to compare the value above with, for example, measured pion or nucleon—Fe absorption cross sections at lower kinetic energy. Interpolating the measured values for 1.4 GeV neutron-nucleus interactions gives for neutrons on iron $\sigma_a = 640 \pm 40$ mb,[7] which is 36 per cent higher than the value determined from Λ. This discrepancy may be ascribed to scattering corrections as well as the nature of the cascade capable of producing the Carbon-eleven reaction, including, e.g. energetic photons.[8]

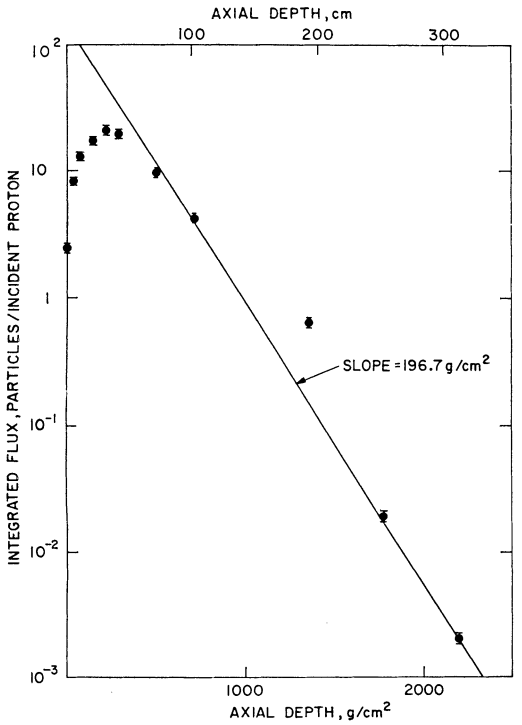

FIG. 10. Total number of energetic particles per incident proton *vs.* depth.

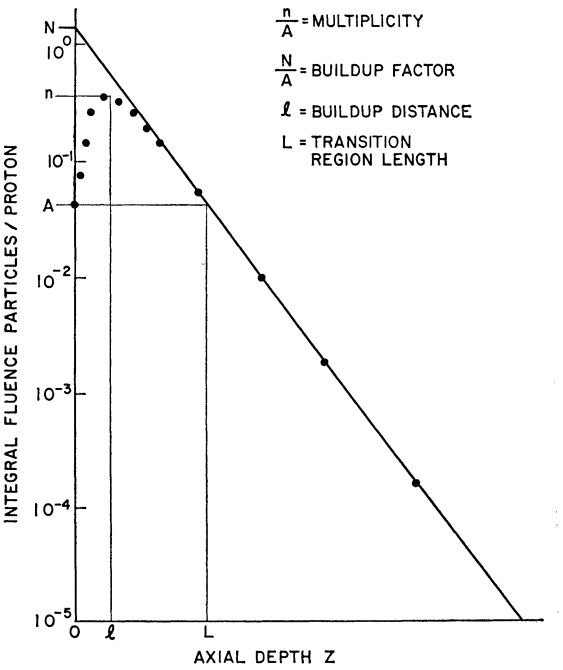

FIG. 11. Schematic definition of some quantities derived from Fig. 10.

TABLE III

Comparison of results from beam stop experiments

Source	Proton beam energy GeV	Detector	Stop mat'l.	λ g/cm^2	Build-up dist. g/cm^2	Transition region length g/cm^2	Λ g/cm^2	Multiplicity	Build-up
Present expt.	28	^{11}C	Fe	156±1.1	230	840	197±3	11.6±0.8	60±4
CERN	18.2	emulsion (tracks)	Fe	120±10	~200	620	185±20	~4	40±10
CERN	18.2	emulsion (stars)	Fe	129	~220	780	185±20	~4	70±20
CERN	18.2	^{11}C	Fe	170	—	—	—	~10	—
CERN	18.2		Conc.	145±10					
CERN	9.1	emulsion (min. tracks)	Fe	119±5	230	460	165±50	~4	~25
CERN	9.1	^{11}C	Fe	145	—	—	—	~9	—
LRL	6.2	^{11}C	Conc.	108	—	—	—	—	—

Some of the results from the present experiment are compared with those from previous studies in Table III. Reasonable agreement is found with the few ^{11}C results available for comparison. The agreement extends to the emulsion data as well, with the notable exception of the peak axial flux attenuation length, λ.

Ranft[9,10] has reported Monte Carlo calculations of the nucleon-meson cascade in steel for protons of incident momentum between 10 GeV/c and 300 GeV/c, finding good agreement between his calculations and the track and star density measurements of Childers *et al.*[2] at 10 GeV/c and by Citron *et al.*[2] at 19.2 GeV/c. At a proton momentum of 30 GeV/c Ranft calculates values of 190 ± 10 g/cm^2 and 195 ± 10 g/cm^2 for the attenuation of the laterally integrated star and track densities respectively. These values are in reasonable agreement with our experimental value of 197 ± 3 g/cm^2 for ^{11}C activity. Comparison with calculated values of the build-up factor is more difficult. Firstly, the build-up factor is extremely sensitive to the attenuation length used to describe the data. Secondly, the particles capable of producing ^{11}C are somewhat lower in energy than those capable of producing stars but higher than those counted as tracks in the calculations due to Ranft. It is gratifying, therefore, to note that our experimental value for a build-up factor of 60 ± 4 is intermediate between the calculated value for tracks of 46 ± 10 and the value for stars of 105 ± 10.

REFERENCES

1. R. H. Thomas, 'Shielding Experiment at 6 GeV,' Lawrence Radiation Laboratory Report UCID 10023 (1964). A. R. Smith, *Proc. 1st Sym. on Accelerator Radiation, Dosimetry and Experience, BNL*, CONF.-651109, November 3–5, 1965, p. 365.
2. J. A. Geibel *et al.*, *Nucl. Instr. and Methods*, **32,** 45 (1965). A. Citron *et al.*, *Nucl. Instr. and Methods*, **32,** 48 (1965). R. L. Childers *et al.*, *Nucl. Instr. and Methods*, **32,** 53 (1965). J. Baarli *et al.*, *Nucl. Instr. and Methods*, **32,** 57 (1965). L. Hoffman and A. H. Sullivan, *Nucl. Instr. and Methods*, **32,** 61 (1965). T. A. Geibel and J. Ranft, *Nucl. Instr. and Methods*, **32,** 65 (1965).
3. G. S. Levine and W. H. Moore, BNL Accel. Dept. Int. Rep. AGSCD-44 (1969).
4. L. N. Blumberg *et al.*, BNL Accel. Dept. Int. Rep. AGS DIV 69–12 (1969).
5. J. B. Cumming, *Ann. Rev. Nucl. Sci.*, **13,** 261 (1963).
6. B. J. Moyer, 'Evaluation of Shielding Required for the Improved Bevatron', Lawrence Radiation Laboratory Report UCRL-9769 (1961); B. J. Moyer, in *Proc. First Int. Conf.—Shielding Around High Energy Accelerators*, Presses Univ. de France, Paris, 1962, p. 65.
7. T. Coor *et al.*, *Phys. Rev.*, **98,** 1369 (1955).
8. L. W. Jones and K. M. Terwilliger, *Phys. Rev.*, **91,** 699 (1953).
9. J. Ranft, *Nucl. Instr. and Methods*, **48,** 133 and 261 (1967).
10. J. Ranft, *Particle Accelerators*, **3,** 129 (1972).

Received 14 September 1972;
in revised form 2 January 1973